Oxidation of guanines in the iron-responsive element RNA: similar structures from chemical modification and recent NMR studies

Suzanne A Ciftan[1], Elizabeth C Theil[2] and H Holden Thorp[1]

Background: The translation or stability of the mRNAs from ferritin, m-aconitase, erythroid aminoevulinate synthase and the transferrin receptor is controlled by the binding of two iron regulatory proteins to a family of hairpin-forming RNA sequences called iron-responsive elements (IREs). The determination of high-resolution nuclear magnetic resonance (NMR) structures of IRE variants suggests an unusual hexaloop structure, leading to an intra-loop G–C base pair and a highly exposed loop guanine, and a special internal loop/bulge in the ferritin IRE involving a shift in base pairing not predicted with standard algorithms.

Results: Cleavage of synthetic 55- and 30-mer RNA oligonucleotides corresponding to the ferritin IRE with complexes based on oxoruthenium(IV) shows enhanced reactivity at a hexaloop guanine and at a guanine adjacent to the internal loop/bulge with strong protection at a guanine in the internal loop/bulge. These results are consistent with the recent NMR structures. The synthetic 55-mer RNA binds the iron-regulatory protein from rabbit reticulocyte lysates. The DNA analogs of the 55- and 30-mers do not show the same reactivity pattern.

Conclusions: The chemical reactivity of the guanines in the ferritin IRE towards oxoruthenium(IV) supports the published NMR structures and the known oxidation chemistry of the metal complexes. The results constitute progress towards developing stand-alone chemical nucleases that reveal significant structural properties and provide results that can ultimately be used to constrain molecular modeling.

Addresses: [1]Department of Chemistry, University of North Carolina at Chapel Hill, Chapel Hill, North Carolina 27599-3290, USA. [2]Children's Hospital of Oakland Research Institute, 747 52nd Street, Oakland, CA 94609, USA.

Correspondence: H Holden Thorp
E-mail: holden@unc.edu

Key words: chemical nuclease, guanine oxidation, iron-responsive element, RNA–protein recognition, RNA structure

Received: **6 August 1998**
Revisions requested: **4 September 1998**
Revisions received: **1 October 1998**
Accepted: **8 October 1998**

Published: **13 November 1998**

Chemistry & Biology December 1998, 5:679–687
http://biomednet.com/elecref/1074552100500679

Introduction

A number of metal-complex reagents oxidize nucleic acids to induce strand scission at sites that can be readily visualized using high-resolution gel electrophoresis [1–3]. If these sites of oxidation can be correlated with structural features of the nucleic acid, then structural information can be obtained quickly from small quantities of material. Such studies are particularly useful and challenging for RNA, which exhibits more demanding oxidation chemistry and more diverse structures than DNA [4–7]. For example, the lack of selective binding of Fe–EDTA to RNA produces a nonspecific cleavage pattern arising from the small, freely diffusible hydroxy radical generated via a Fenton reaction [2]. Using this oxidant, the solvent-protected sites for the 160 nucleotide P4–P6 domain of *Tetrahymena thermophila* were observed and were predicted to lie within a helix–helix folding boundary [8]. This folding was later confirmed by the determination of the crystal structure, which resolved specific interactions between the P5 tetraloop and the P6 bulge receptor [9]. We have developed a related approach based on $Pt_2(pop)_4^{4-}$, which does not bind to polyanions and abstracts hydrogen atoms directly from DNA sugars [10]. A complementary approach is to use an oxidant with a selective binding affinity for certain structural features. For example, the $Rh(phen)_2phi^{2+}$ (phen = 1,10-phenanthroline; phi = 9,10-phenanthrenequinone diimine) reaction is selective for distorted regions within compact RNA structures where intercalation is favored [4,11,12].

Metal complexes that cleave nucleic acids often act by sugar oxidation, as in the examples discussed above, and also by base oxidation, usually at guanine. Burrows and Rokita [5] have developed a family of nickel complexes that catalyze the oxidation of guanines by persulfate with a strong selectivity for single-stranded and mismatched guanines [5]. We have developed a system based on the complex $Ru(tpy)(bpy)O^{2+}$ (tpy = 2, 2′, 2″-terpyridine, bpy = 2, 2′ bipyridine) that oxidizes guanine in DNA and RNA without a sacrificial oxidant and with a preference for solvent-accessible sites [13,14]. With DNA, the complex also oxidizes the 1′ hydrogen; the 2′-OH deactivates the 1′-C-H bond, however, so guanine oxidation is observed almost exclusively in RNA [15,16]. The oxidation preferences for $Ru(tpy)(bpy)O^{2+}$ have been mapped in duplex DNA, single-stranded DNA, DNA and RNA hairpins, and tRNA [13,14].

The binding of cationic transition metal complexes such as $Ru(tpy)(bpy)O^{2+}$ to nucleic acids has been studied extensively [17–19]. In particular, the ability of complexes

containing certain conjugated organic ligands to intercalate in DNA or RNA is an intriguing issue [20]. Large planar ligands such as dipyridophenazine (dppz) clearly can be used to generate octahedral metal complexes that bind to DNA by classical intercalation, as is evident in viscometry assays and in nonelectrostatic binding affinities [19,21]. The oxoruthenium(IV) complex of dppz also appears to intercalate into semi-denatured tRNA, but not the fully folded form, as observed for ethidium [14]. In contrast, the simple Ru(tpy)(bpy)O^{2+} complex contains no organic ligands that are more extended than one six-membered aromatic ring, so there is no extended flat surface to intercalate into nucleic acids. Accordingly, the binding affinity of Ru(tpy)(bpy)O^{2+} can be rigorously attributed solely to electrostatic binding of the dicationic complex to nucleic-acid polyanions [22]. Furthermore, comparison of cleavage patterns of Ru(tpy)(bpy)O^{2+} and the intercalating dppz analog show that the sites attributable to intercalation are all absent with Ru(tpy)(bpy)O^{2+}. As the electrostatic binding is relatively nonspecific, the studies here with the iron-responsive element (IRE) and Ru(tpy)(bpy)O^{2+} show the effects only of the accessibility of the oxidized site in the nucleic acid.

The translation or stability of ferritin, m-aconitase, erythroid aminoevulinate synthase and the transferrin receptor mRNAs is controlled by the binding of two iron regulatory proteins (IRP1 and IRP2) to the 5′- or 3′-untranslated region of the corresponding mRNAs [23–25]. The regulatory proteins bind a family of hairpin-forming RNA sequences called iron-responsive elements; for example, IRP binding to the ferritin mRNA suppresses ferritin synthesis and consequently iron storage at low cellular iron concentrations. The IREs contain a highly conserved 5′-$CAG_{16}UG_{18}X$ hexaloop (where X is C, A or U) and either a one-base bulge or, in the case of ferritin, an internal loop/bulge. The IRE sequence from bullfrog ferritin H-chain (IRE-30R) is shown in Figure 1. There is also an internal loop/bulge comprising UG7C/C in the bullfrog ferritin H-chain sequence that is a simple one-base C bulge in most other IREs. Recent studies suggest ferritin IRE-specific internal loop/bulge influences IRP2 binding and the relative expression of ferritin over the other IRP-regulated proteins [26].

The structure of the IRE has been studied extensively using nuclear magnetic resonance (NMR) [27–29]; there are two important structural features discerned in these studies that are relevant here. First, the hexaloop contains two guanines, one of which (G18) is observed, using NMR, to base pair with C14 found across the loop to form a more stable, extended helix [27–29]. Second, there is a rearrangement in the base pairing around the UGC/C internal loop/bulge for the ferritin H-chain sequence [27]. Secondary structure calculation using the 'm-fold' program [30] predicts that the folded structure will be that shown in Figure 1, where the UGC and C are unpaired; NMR studies, however, support

Figure 1

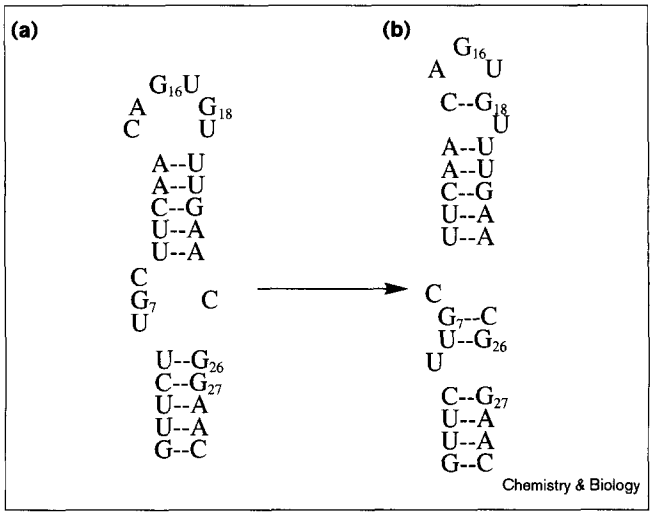

Secondary structure of IRE **(a)** predicted by m-fold and **(b)** observed by NMR. Figure adapted from [27].

formation of a G7–C25 base pair and a U6–G26 wobble pair, leaving single-base bulges at C8 and U5 [27]. The U6–G26 wobble pair is classified as 'dynamic' on the basis of NMR data showing two G–U base pairs with pH-dependent conformations involving U5–G26 and U6–G26. Other pertinent structural features in the NMR structures are a high degree of solvent exposure for the hexaloop guanine that is not base paired (G16) [29] and a cation-binding site near the UGC/C bulge [27]. The alternative base pairing determined from NMR studies is shown in Figure 1.

The NMR structures are supported by a number of chemical and biochemical results. Pairing of G18 and C14 is supported by mutations in the conserved IRE sequence that eliminate protein binding, such as a single base deletion at C14 [31] or a G18→A mutation [12], and by *in vitro* evolution studies that show high-affinity binding by the double mutant (5′-$UAG_{16}UA_{18}N$-3′), which can also base pair across the loop [32]. Oxidation by Fe–EDTA produced protected sites mostly on the 5′ side of the hairpin, possibly as a result of folding at the internal loop/bulge [33]. Most dramatically, when the 900-base full-length IRE transcript was oxidized by Ru(tpy)(bpy)O^{2+}, the only modification detected was at G16, implying high solvent exposure at this site [12]. Oxidation by $Cu(phen)_2^+$ in the internal loop/bulge was inhibited by Mg^{2+}, supporting the existence of a cation-binding site in this region [33], and *in vitro* selection studies also supported base pairing of G7 and C25 [34].

We report here on studies of the 30-mer and 55-mer IREs and their DNA analogs (Figure 2) using Ru(tpy)(bpy)O^{2+}. The synthetic 55-mer RNA was shown to bind the IRP by gel mobility shift. The primary site of oxidation in the RNA is at G16, as observed in the full-length transcript

Figure 2

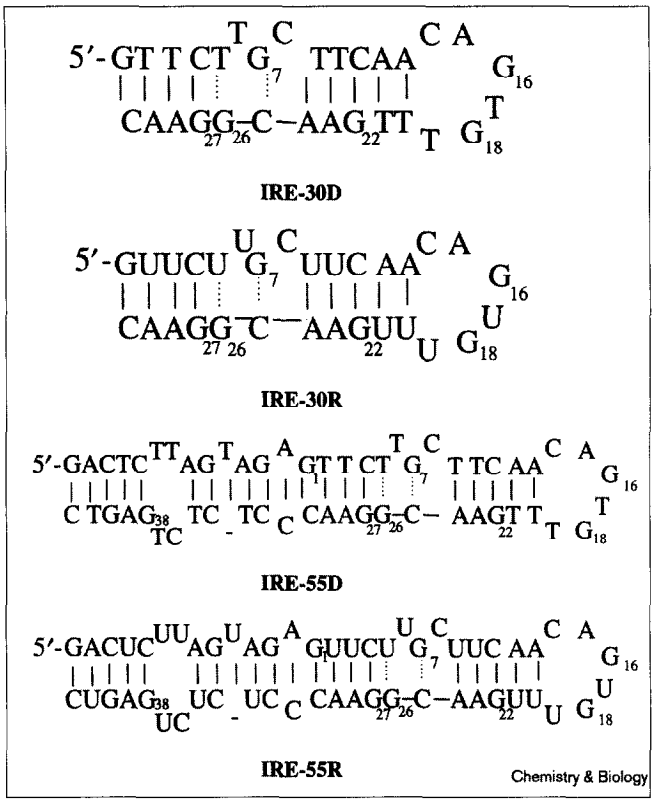

DNA and RNA sequences used in this study.

Figure 3

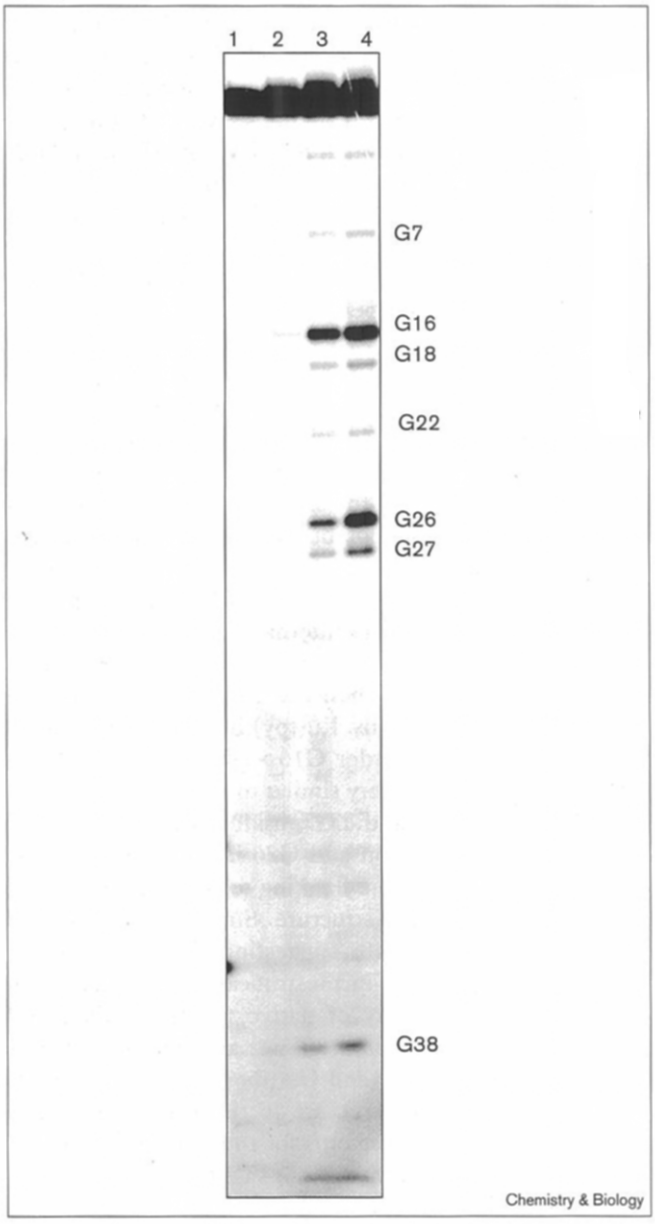

Autoradiogram of a 20% polyacrylamide sequencing gel for the 3′-^{32}P-labeled IRE-55R sequence showing the guanine reactivity with increasing Ru(tpy)(bpy)O^{2+} in 4 mM sodium phosphate buffer (pH 7) and 1 μg of carrier tRNA. Lane 1, RNA control; lanes 2–4, 6, 18 and 30 μM Ru(tpy)(bpy)O^{2+}.

[12]. The cleavage pattern in the loop is consistent with the formation of the G18–C14 base pair. The cleavage pattern in the internal loop/bulge shows little reactivity at G7 and a very strong site at G26, also as expected from the NMR results. Cleavage patterns for the DNA analogs support these findings. Taken together, the relationship of the chemical modification and NMR studies suggest new avenues for discerning alternative secondary structures in RNA hairpins based on cleavage patterns. These studies could ultimately allow determination of secondary structures directly from the cleavage patterns on small quantities of biologically relevant RNAs.

Results

RNA oxidation

The initial sequence studied was IRE-55R, shown in Figure 2, that contains the 30-base conserved IRE region plus a base-paired flanking region that has been identified in the ferritin message [25]. This 55-mer was chosen because it was suspected to be the minimal sequence needed to bind the IRP. Indeed, the 55-mer was shown to bind the IRP from rabbit reticulocyte lysate by gel mobility shift. Addition of rabbit reticulocyte lysate to the radiolabeled 55-mer produced a RNA–protein complex that was visualized as a higher molecular weight band on a native gel than the 55-mer. The effects of proteinase K, heparin and β-mercaptoethanol on the RNA–protein complex were all as expected for the IRE–IRP [35]. Studies of the synthetic 55-mer are therefore relevant to understanding the native RNA–protein recognition.

The cleavage pattern for oxidation of the IRE-55R by Ru(tpy)(bpyy)O^{2+} is shown in Figure 3. In RNA, oxidation is seen almost solely at guanine nucleotides, because the

reactivity at the ribose moiety is poor [16]. The G16 site in the hexaloop was oxidized to the largest extent, as observed for the 900-nucleotide sequence [12]. Other sites were oxidized in the order G26 > G27 > G18 ~ G22 ~ G7. This pattern of oxidation is consistent with the expectations from the secondary structure shown in Figure 1. The low reactivity of G7 and high reactivity of G26 support the formation of a stable G7–C25 base pair and a dynamic U6–G26 wobble pair. Likewise, the much greater oxidation of G16 than G18 is consistent with the formation of the C14–G18 base pair. These points are discussed in relation to detailed models below.

The nucleotides on either side of the 30-mer conserved region of the IRE form a base-paired stem termed the flanking region [12]. Mutations in the flanking region disturb the extent of regulation of ferritin synthesis, alter a site near the junction of the stem and terminal loop that is cleaved by iron bleomycin, but do not influence IRE–IRP binding as assessed by gel mobility shift [36]. To determine whether the flanking region influences the primary features of the hexaloop or internal loop/bulge, a truncated RNA 30-mer was prepared containing only the IRE itself (IRE-30R; Figure 2). When the IRE-30R sequence was subjected to oxidation by Ru(tpy)(bpy)O^{2+}, the cleavage pattern followed the order G16 > G26 > G18 ~ G22 ~ G7 (Figure 4), which was very similar to that for the IRE-55R sequence. In particular, the G7 residue is still very strongly protected from oxidation and G26 is quite reactive, suggesting that removing the flanking region does not disrupt the internal loop/bulge structure. Similarly, G16 is much more reactive than G18, suggesting that the hexaloop structure is maintained in the truncated sequence. Comparison of the reactivity of native ferritin mRNA, full-length transcript, and both 30-mer and 55-mer synthetic RNAs with RNAse T1 and $Cu(phen)_2^+$ also showed the retention of the IRE structure in the isolated sequence [33,37]. The cleavage patterns for the IRE-30R and IRE-55R oligomers are summarized in Figure 5a.

Figure 4

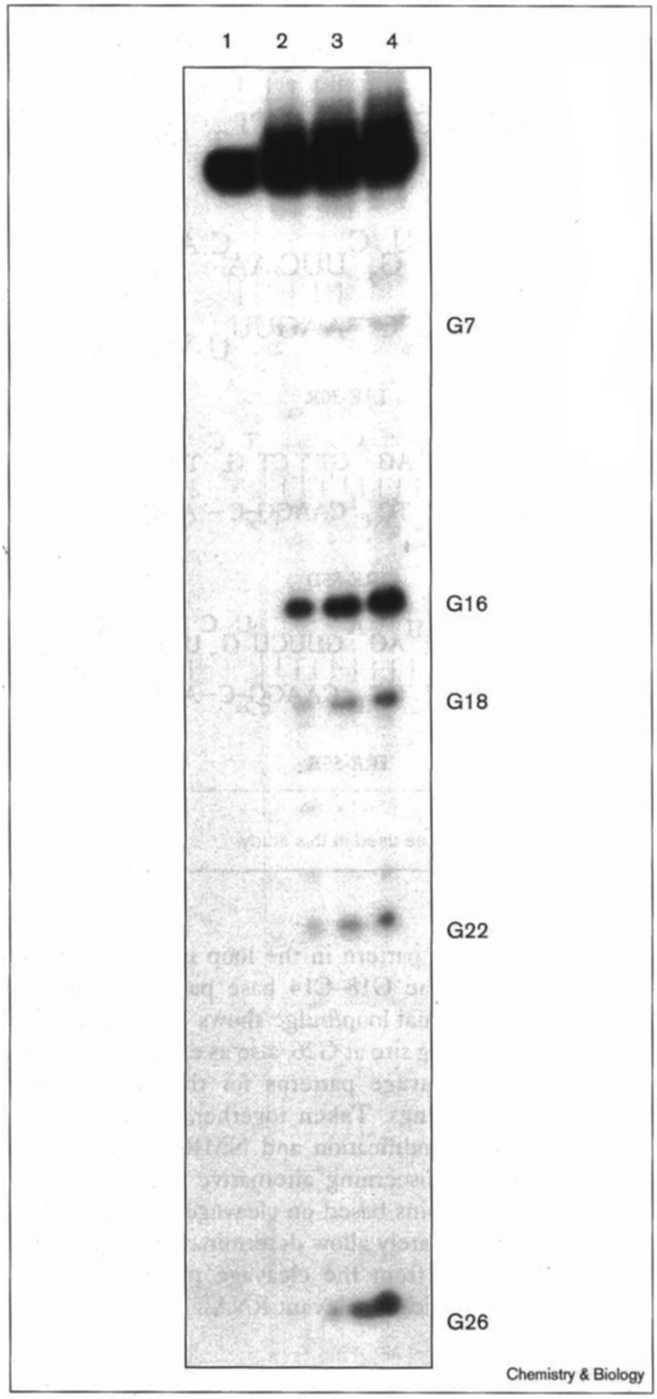

Autoradiogram of a 20% polyacrylamide sequencing gel for the 3′-^{32}P-labeled IRE-30R sequence showing the guanine reactivity with increasing Ru(tpy)(bpy)O^{2+} in 25 mM sodium phosphate buffer (pH 7) and 2 μg carrier tRNA. Lanes 1–4, 0, 18, 24 and 30 μM Ru(tpy)(bpy)O^{2+}.

DNA analogs

The parallel study of RNAs and their DNA analogs has been used to advantage recently in chemical cleavage studies. For example, studies of tRNA and tDNA analogs suggest similar folding in the two species [38,39], and studies of TAR RNA and its DNA analog have helped elucidate the binding of intercalators selectively to the bulge region [14,40]. For cleavage agents that damage nucleic acids at the sugar moiety, an advantage of DNA analogs is that sugar oxidation is much easier and leads to better defined products than in RNA. Although base pairing is similar in both DNA and RNA, the effects of the sugar conformation are dramatic. So when a cleavage pattern for an RNA is compared with that of its DNA analog, the reactivity pattern that arises simply because of the sequence context can be more readily assessed. If a particular pattern is distinct for the RNA, then it can be more confidently assigned to a geometric origin. For example, we believe the relationship between the cleavage intensities of G16 and G18, and those of G7 and G26 are a consequence of the

Figure 5

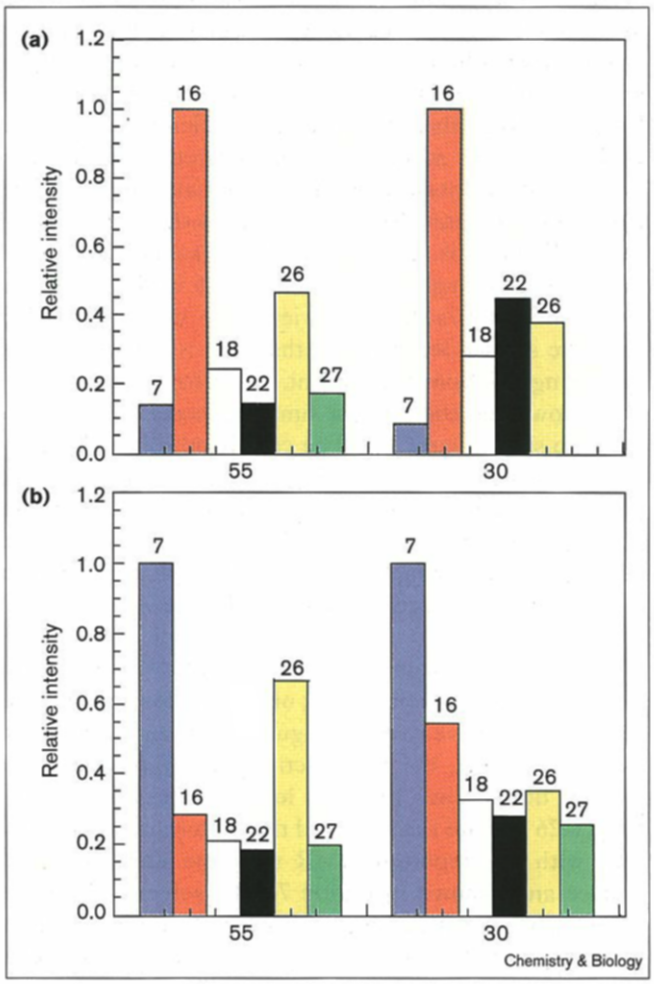

(a) The relative cleavage intensities for the IRE-55R and IRE-30R reactions with Ru(tpy)(bpy)O^{2+}, showing the extent of cleavage at G7 (blue), G16 (red), G18 (white), G22 (black), G26 (yellow) and G27 (green). Intensities are normalized to the intensity of G16 for each oligomer. Errors from multiple trials are ± 20%. **(b)** Relative intensities for cleavage of the IRE-55D and IRE-30D oligomers by Ru(tpy)(bpy)O^{2+}; color scheme, errors and normalization are the same as in (a).

RNA conformation. We would therefore not expect to see these same patterns in the DNA analogs, whose helix, loop and folding geometries are very different. In the DNA analogs, dT is substituted for rU, which is a significant perturbation in the IRE because of the large number of G–U wobble pairs. This consideration is probably more important here than in the DNA analogs of tRNA and TAR RNA studied previously [13,38–40], where there are less significant G–U wobble pairs.

The stability of the folded structures of the IRE-30D and the IRE-55D shown in Figure 2 was assessed by thermal denaturation. The measured T_m values for the IRE-30D and the IRE-55D sequences were 46°C and 41°C in pyrophosphate buffer (pH 7), respectively. For reference, the T_m value for the IRE-30R is 52°C in 100 mM phosphate buffer (pH 6.9) [41]. So, in DNA, the flanking region actually decreased the stability of the IRE. Nevertheless, the guanines in the flanking region were not particularly reactive towards Ru(tpy)(bpy)O^{2+}, suggesting that the flanking region is base paired in the DNA analog.

The cleavage patterns obtained upon oxidation of the IRE-55D and IRE-30D oligomers by Ru(tpy)(bpy)O^{2+} are shown in Figure 5b. These changes affect the accessibility of G7, indicating a change in the conformation of the internal loop/bulge probably due to a disruption of the G7–C25 base pair. Furthermore, the preference for G16 is lower than in the DNA analogs, suggesting that the loop geometry is different from that of the RNAs. As neither G16 nor G18 in the terminal loop of IRE-30D or IRE-55D is as accessible as G7, the terminal loop might be more disordered than the internal loop. Alternatively, an A–T base pair might form in the terminal loop of the DNA analogs. The greater stability of G–U wobble pairs in RNA than G–T mismatches in DNA is no doubt an important factor.

IRP binding of IRE-55D was tested using a crude cell extract (rabbit reticulocyte lysate) as a source of natural IRP-1 and IRP-2, and the change in gel mobility of labelled DNA as an indication of protein binding. Earlier studies showed that purified IRP-1 did not bind to IRE-55D [33]. A protein–IRE-55D complex (proteinase k sensitive and heparin resistant) was, in fact, observed. Reducing agent did not change the fraction of DNA bound in the manner expected for the IRP [35] and the IRE-55R did not disrupt the complex of the DNA analog, however. Moreover, the IRE-55D–protein complex had a very different mobility than the IRE-55R–IRP complex under the same conditions. It therefore appears that there is an IRP-independent IRE-55D–protein complex that forms in rabbit reticulocyte lysate, but whether such a complex forms in the nucleus, when the IRE sequence is in a single-stranded form, is unknown.

Discussion

Correlation of NMR structure and guanine oxidation

The results of guanine oxidation with Ru(tpy)(bpy)O^{2+} are well-supported by the recent NMR studies on IRE. The first result of interest is our earlier observation [12] that in the full-length natural message the only observed site of oxidation in the IRE or flanking region was at G16. This result suggested a high degree of solvent exposure for G16 that was later confirmed by NMR. First, Laing and Hall [28] published a study confirming the C14–G18 base pair, and later, Addess *et al.* [29] published the coordinates of a more complete NMR structure of the hexaloop and neighboring base pairs, shown in Figure 6. As seen in Figure 6, G16 sits on top of the hexaloop and is projected well into the solvent. The studies reported here are consistent both with our earlier result on the full-length message and with

Figure 6

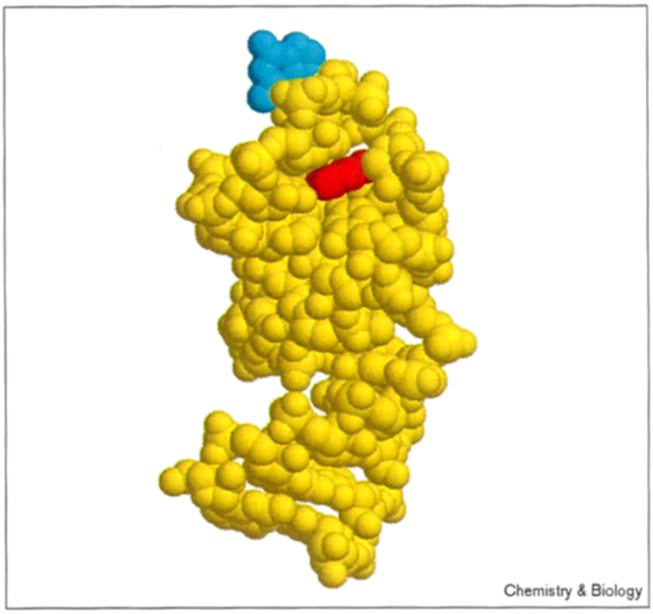

Structure of IRE with only a single-base C bulge determined by Addess *et al.* [29] using NMR. The solvent accessible G16 in the hexaloop is shown in blue and the less reactive hexaloop guanine (G18) is shown in red. Coordinates taken from [29] (accession code 1AQO). Solvent-accessible surface areas for the guanine bases in the structure were: G7 (30 Å^2), G16 (186 Å^2), G18 (41 Å^2) and G22 (44 Å^2).

the NMR structure in showing that G16 is the most reactive site in both the 30-mer and 55-mer IRE sequences and that G18 is much less reactive than expected for a single-stranded guanine. The solvent-accessible areas calculated for the guanine bases are 186 Å^2 for G16 and 30–45 Å^2 for the other guanines, which correlate well with the high reactivity of G16 seen with Ru(tpy)(bpy)O^{2+}.

Earlier studies showing that only G16 was cleaved were performed on the full-length ferritin mRNA and cleavage sites were determined using primer extension analysis [12]. The extra sites observed here (Figures 3 and 4) can be attributed to the effective increase in oxidant concentration compared with the total number of nucleotides present in the shorter RNAs or to modifications that were transparent to the reverse transcriptase/primer extension analysis used with the full-length RNA. Alternatively, long-range interactions in the full-length RNA might block all sites except G16.

The cleavage pattern observed in the internal loop/bulge of the IRE correlates well with the recent NMR structure of the ferritin IRE sequence determined by Gdaniec *et al.* [27] and indicates a different structure than that of the consensus IRE with the internal single-base C bulge determined using NMR [29]. The recent determination of the structure by Gdaniec *et al.* [27] showed in detail the UGC/C internal loop bulge and found a stable G7–C25 base pair that situates G7 in the interior of a folded A-type helix. This conformation places the G26 residue in a dynamic U6–G26 wobble pair that displays pH-dependent conformational heterogeneity. One structure of the internal loop/bulge from Gdaniec *et al.* [27] is shown in Figure 7. Note that the cleavage studies reported here were performed at pH 7, so the degree to which the dynamic pair is intact might not be the same as in the low pH NMR structures. Nevertheless, even though the structure in Figure 7 is one in which the dynamic base pair is intact, G7 is strongly protected and G26 is highly solvent exposed. Figure 7a shows the view from 'underneath' G26 from the stem side, revealing that G26 is exposed and is protecting G7 from the solvent. Rotating the hairpin by 180° shows that there is not similar exposure of G7 from the loop side (Figure 7b). The calculated solvent accessibilities for the guanines in Figure 7 give a significantly higher degree of exposure for G26 than for G7 when the accessible surface areas are calculated either for the entire nucleotides (including the sugar and phosphate) or for the nucleobases alone (see the legend to Figure 7).

The cleavage pattern for Ru(tpy)(bpy)O^{2+} shows an unusually low reactivity at G7, one of the lowest levels of reactivity we have seen at a guanine in an oligomer of this size. In fact, the low reactivity at G7 parallels that seen at buried sites in much longer tRNAs [14]. Similarly, G26 is quite reactive, and the pattern is very consistent with the reported NMR structure and accessible surface areas shown in Figure 7. The solvent-accessible surface areas for the guanines in Figure 7 are in the order G16 > G26 > G22 ~ G7 ~ G18, which is the same trend observed for cleavage by Ru(tpy)(bpy)O^{2+} (Figure 5a).

Targeting of cleavage by Ru(tpy)(bpy)O^{2+} at the internal loop/bulge (G26) could represent a more general metal–RNA interaction site. For example, Mn^{2+} efficiently inhibited oxidation of G26 by Ru(tpy)(bpy)O^{2+} [42]. In addition, recent NMR studies show a strong binding site for cobalt(III) hexammine near G26 that stabilizes the dynamic U6–G26 base pair [27]. Thus, the selective quenching of oxidation at G26 by Mn^{2+} probably arises from a combination of preferential binding of Mn^{2+} to that site (and therefore more efficient Mn^{2+} quenching of Ru(tpy)(bpy)O^{2+}) and stabilization of the G26 base pair, rendering the site less solvent accessible. This observation parallels the Mg^{2+} inhibition of cleavage by $Cu(phen)_2^+$ at this site observed previously and supports the assertion that physiologically significant metal ions bind near G26 [37].

The results on the DNA analogs of the ferritin IRE further confirm the special folding at the internal loop/bulge. In contrast to the RNA results, strong cleavage of the DNA analogs by Ru(tpy)(bpy)O^{2+} is observed at G7. The presence of G–U pairs, the sugar conformation of the ribose groups and the associated A-type helix must lead to

Figure 7

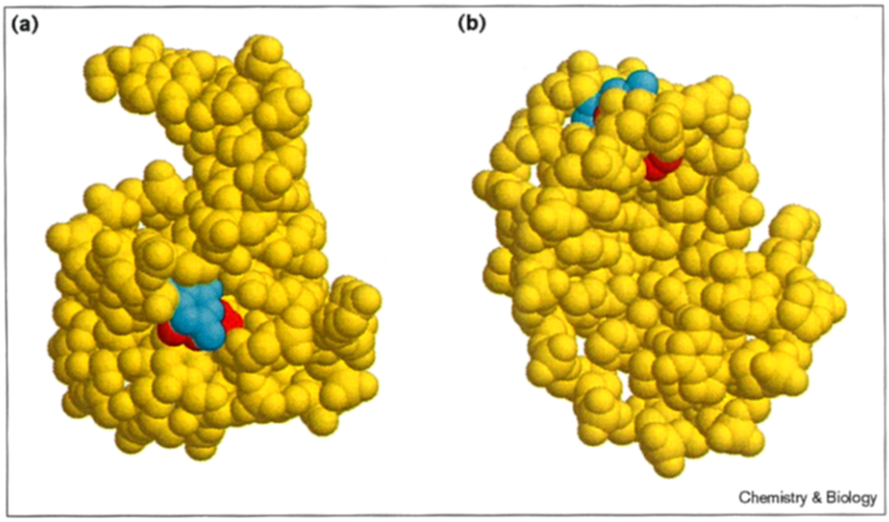

Structure of IRE with the UGC/C internal loop/bulge determined by Gdaniec *et al.* [27] using NMR. The reactive G26 is shown in blue and the buried G7 is shown in red. Coordinates taken from [27]. Solvent-accessible surface areas for the guanine nucleotides and bases in the structure were: G7 (163 Å^2, entire nucleotide; 43 Å^2, base only), G16 (255, 126 Å^2), G18 (170, 58 Å^2), G22 (185, 36 Å^2) and G26 (220, 66 Å^2). Considering the areas for either the entire nucleotides or the base only gives the observed order: G16 > G26 > G22 ~ G18 ~ G7. **(a)** View from the stem side of the internal loop/bulge showing the exposed face of G26. **(b)** View from the loop side of the internal loop/bulge showing that the opposite face of G7 is not exposed.

the folding observed in the internal loop/bulge. This finding supports our observation that a guanine adjacent to the internal loop in the TAR RNA is somewhat protected from cleavage by Ru(tpy)(bpy)O^{2+} but quite reactive in the DNA analog [14]. The distinct structure of the IRE-55D sequence is reflected in the inability of the IRP to bind and the recognition of the IRE-55D by another protein in rabbit reticulocyte lysate.

Prospects for chemical nucleases as stand-alone structural tools for RNA

The advantages of chemical nucleases have been described previously in several other papers [1,2,4–6]. The primary advantage of chemical nuclease studies is that the experiments can be conducted on small quantities of radiolabeled nucleic acid, whereas NMR and crystallography studies require much larger quantities of material. Additional advantages of cleavage studies are that it is straightforward to screen mutant nucleic acids for structural changes, and the studies can usually be conducted in solution under native conditions, which is often an advantage over solid-state crystallography. Chemical nuclease experiments, however, provide only a series of cleavage bands that must then be related to the entire structure rather than a complete structure (as in crystallography) or in a series of constraints that can be used to model the structure (as in NMR). Ultimately, chemical nucleases must be developed that provide a set of constraints similar to that derived from NMR that can be used to model the total structure.

The first step towards developing stand-alone structural tools for RNA based on chemical nucleases is to understand the cleavage patterns of the different reagents for complex RNAs whose structures are known. The prototype system for these studies has been tRNA, and the cleavage pattern for most chemical nucleases in wide use has been determined for tRNA and compared with the crystal structure [14,43–45]. In a particularly compelling case, nickel complexes that damage distorted guanines give cleavage patterns that quantitatively predict the solvent accessibilities determined from the known structure [34].

In large RNAs and RNA–protein complexes, chemical cleavage studies (usually with Fe–EDTA) have been used to determine sites of tertiary protection in the nucleic acid itself or sites of protection by protein [8,33]. These studies have met with great success in predicting relatively low-resolution structures of very large molecular assemblies such as the ribosome and the tetrahymena ribozyme [8,46,47]. Here, we consider a different question of structural studies at higher resolution on smaller RNAs [48–50], such as the IRE. Such studies were first suggested by Sigman and coworkers [45] upon showing that Cu(phen)$_2^+$ prefers single-stranded loops in RNA hairpins. The system that is similar to the IRE that has been studied extensively is the TAR RNA, where the structure of the internal loop has been related to its chemical reactivity towards a variety of chemical nucleases, mostly in light of recent NMR structures [11,14,40,51].

Here we have shown that the two distinguishing features of the ferritin IRE are apparent in the cleavage pattern, namely the C14–G18 base pair and the associated hexaloop structure, and the G7–C25 base pair and the associated structure of the internal loop/bulge. In the former case, the high reactivity of G16 compared to G18 was determined in the natural message without the benefit of a high-resolution NMR structure [12], and the origin of this result is now strikingly apparent in Figure 6. Here we analyze the internal loop/bulge structure with the benefit of the NMR studies of Gdaniec *et al.* [27], and the cleavage studies nicely support the proposed structure in Figure 7. Certainly

one reason why many cleavage studies have been mostly confirmatory of other high-resolution methods is that there have been a relatively small number of systems of interest (such as TAR and the IRE), although a rapid proliferation of these systems can now be anticipated based on the increase in availability of RNA sequence data and on results from *in vitro* selection of therapeutically active aptamers [52]. To characterize many of these upcoming systems requires further optimization and discovery of chemical cleavage agents and the principles governing the relationship of their cleavage patterns and the implied biomolecular structure.

Significance

Translation and stability of the mRNAs for a number of proteins related to iron metabolism are controlled by binding of two regulatory proteins to a hairpin-forming family of RNA sequences called the iron-responsive elements (IREs). Conformational dynamics in IRE produces an unexpected pattern of solvent accessibility in guanine bases near two loops that are bridged by conserved G–C base pairs. Oligoribonucleotides based on IRE were reacted with transition metal complexes based on oxoruthenium(IV) that have been designed to oxidize guanine bases in RNA with a selectivity that arises primarily from solvent accessibility. The oxoruthenium reagent induces aniline-labile strand scission selectively at G16, which is a residue in the IRE hairpin loop. The high solvent accessibility of G16 is a result of the base pair in the terminal loop between another guanine (G18) and cytosine (C14). The oxoruthenium reagent selectively oxidizes G16 in both the short oligomers (30 nucleotides) and the full-length RNA (1000 nucleotides). Another reactive site in the oligomers is G26, which is near the internal loop/bulge and becomes solvent-exposed because of the conformational dynamics of the loop/bulge. The solvent accessibility pattern for all of the guanines in the oligomers is the same when calculated from high-resolution nuclear magnetic resonance (NMR) structures or obtained from the cleavage pattern with oxoruthenium(IV). This observation indicates that the cleavage reaction provides a simple means for determining whether the folded RNA structure is present, as has been shown in the IRE model, and could be used for other natural and mutant RNAs under a wide variety of conditions.

Materials and methods

Metal complex

The metal complex Ru(tpy)(bpy)O^{2+} was synthesized as the aquaruthenium(II) complex and electrochemically converted to the reactive oxoruthenium(IV) form as described previously [15].

Gel mobility shift

Nuclease-treated rabbit reticulocyte lysate (Promega), the radiolabeled oligonucleotide, and low-molecular-weight heparin (Sigma) were mixed and incubated at room temperature for 5–30 min. Treatment of the mixture with proteinase K (Promega) required incubation at 37°C for 30 min. Products were visualized on a native gel.

Oligodeoxynucleotide cleavage

The oligodeoxynucleotides d(5′-TTCAACAG$_{16}$TG$_{18}$TTTG$_{22}$AA), d(5′-GTTCTTG7TTCAACAG$_{16}$T G$_{18}$TTTG$_{22}$AACG$_{26}$ G$_{27}$AAC), and d(5′-GACTCTTAGTAGAGTTCTTG$_7$TTCAACAG$_{16}$TG$_{18}$TTTG$_{22}$AACG$_{26}$ G$_{27}$AACCCTCTCTGAGTC) were purchased from the Oligonucleotide Synthesis Center in UNC-CH Department of Pathology and were purified by gel cutting. 5′–^{32}P labeled sequences were prepared from 5′-[γ–^{32}P]-dATP (Amersham) and T4 polynucleotide kinase (New England Biolabs). Approximately 1 mg of Ru(tpy)(bpy)O^{2+} was dissolved into 10 ml of purified water to form a stock solution of oxidant. A typical reaction consisted of 0–10 µl of oxidant, 2 mM sodium phosphate buffer (pH 7), 4 µl unlabeled oligodeoxynucleotide and 20–25,000 cpm of radiolabeled oligodeoxynucleotide. Oxidation was allowed to proceed over a period of 5 min by addition of 25 µl Ru(tpy)(bpy)O^{2+} and the reaction was quenched with 10 µl of 95% ethanol. All DNA reactions were treated with 60 µl of 0.7 M piperidine at 90°C for 30 min. The cleavage intensities were measured by scanning the Kodak Biomax MR X-ray film using a Macintosh OneScanner equipped with Ofoto 2.0, integrated using the NIH Image 1.52 software, and analyzed using Kaleidagraph software.

Oligoribonucleotide reactions

RNA was synthesized by *in vitro* transcription. For example, the DNA template for IRE-30R d(5′-TAATACGACTCACTATAGCAAGAACGAAGTTGCACAAACT TGCCTTG) was annealed in 10% excess to the T7 polymerase promoter oligonucleotide d(5′-CTATAGTGAGTCGTATTA) in 10× concentrated T7 polymerase buffer (New England Biolabs). The primer–template hybrid was added to 3 µl of NTP (Life Technologies), mixed with 1 µl T7 polymerase (New England Biolabs) per µg of template DNA and incubated at 37°C for 3 h. The resulting RNA oligonucleotide was separated from the DNA template and promoter by gel cutting. The 55-mer transcript was synthesized in an analogous fashion. The RNA was labeled with 3′-[γ-^{32}P]-pCp (NEN, DuPont) using T4 ligase (Boehringer Mannheim) and was purified by gel cutting. The oxidation reactions were performed in an analogous fashion as the oligodeoxynucleotide reactions. Base treatment required 20 µl of 1.0 M aniline (pH 4.5) at 60°C for 20 min. Care was taken to use an RNase-free environment.

Thermal denaturation

Absorption at 260 nm was monitored as a function of temperature using the kinetic program of the Hewlett-Packard UV-Vis Diode-Array Spectrophotometer. The solution sample was placed in a 1 cm pathlength quartz cell equipped with a thermal jacket and an ethylene glycol/water temperature bath controller. The temperature was measured using a Physitemp Type IT-18 thermocouple and a Baxter Digital thermometer. Melting curves were analyzed using Kaleidagraph software, and the average of the pre- and post-denaturation absorption values was used to determine the melting temperature.

Acknowledgements

We gratefully acknowledge the National Science Foundation (H.H.T.) and the National Institutes of Health (E.C.T.) for support. H.H.T. is an Alfred P. Sloan Research Fellow and a Camille Dreyfus Teacher-Scholar. We thank L.G. Pedersen for helping with the solvent accessibility calculations and A. Pardi for providing coordinates prior to publication.

References

1. Thorp, H.H. (1995). Electron-, energy-, and atom-transfer reactions between DNA and metal complexes. *Adv. Inorg. Chem.* **43**, 127-177.
2. Draganescu, A. & Tullius, T.D. (1996). Targeting of nucleic acids by iron complexes. *Metal Ions Biol. Syst.* **33**, 453-484.
3. Sigman, D.S., Landgraf, R., Perrin, D.M. & Pearson, L. (1996). Nucleic acid chemistry of the cuprous complexes of 1,10-phenanthroline and derivatives. *Metal Ions Biol. Syst.* **33**, 485-514.
4. Chow, C.S. & Barton, J.K. (1992). Transition metal complexes as probes of nucleic acids. *Methods Enzymol.* **212**, 219-241.
5. Burrows, C.J. & Rokita, S.E. (1994). Recognition of guanine structures in nucleic acids by nickel complexes. *Acc. Chem. Res.* **27**, 295-301.
6. Theil, E.C. (1994). Transition metal coordination complexes as probes of mRNA structure: the IRE (Iron Recognition Element) of ferritin mRNA as a case study. *New J. Chem.* **18**, 435-441.

7. Battigello, J.-M., Cui, M. & Carter, B.J. (1996). RNA recognition and cleavage by iron(II)bleomycin. *Metal Ions Biol. Syst.* **33**, 593-618.
8. Celander, D.W. & Cech, T.R. (1991). Visualizing the higher order folding of a catalytic RNA molecule. *Science* **251**, 401-407.
9. Cate, J.H., *et al.*, & Doudna, J.A. (1996). Crystal structure of a group I ribozyme: principles of packing. *Science* **273**, 1678-1685.
10. Breiner, K.M., Daugherty, M.A., Oas, T.G. & Thorp, H.H. (1995). An anionic diplatinum DNA photocleavage agent: chemical mechanism and footprinting of lambda repressor. *J. Am. Chem. Soc.* **117**, 11673-11679.
11. Neenhold, H.R. & Rana, T.M. (1995). Major groove opening at the HIV-1 tat binding site of TAR RNA evidenced by a rhodium probe. *Biochemistry* **34**, 6303-6309.
12. Thorp, H.H., McKenzie, R.A., Lin, P.-N., Walden, W.E. & Theil, E.C. (1996). Cleavage of functionally relevant sites in ferritin mRNA by oxidizing metal complexes. *Inorg. Chem.* **35**, 2773-2779.
13. Carter, P.J., Cheng, C.-C. & Thorp, H.H. (1996). Oxidation of DNA hairpins by oxoruthenium(IV): effects of sterics and secondary structure. *Inorg. Chem.* **35**, 3348-3354.
14. Carter, P.J., Cheng, C.-C. & Thorp, H.H. (1998). Oxidation of DNA and RNA by oxoruthenium(IV) metallointercalators: visualizing the recognition properties of dipyridophenazine by high-resolution electrophoresis. *J. Am. Chem. Soc.* **120**, 632-642.
15. Cheng, C.-C., *et al.*, & Thorp, H.H. (1995). Relative rates and potentials of competing redox processes during DNA cleavage: oxidation mechanisms and sequence-specific catalysis of the self-inactivation of oxometal oxidants. *J. Am. Chem. Soc.* **117**, 2970-2980.
16. Neyhart, G.A., Cheng, C.-C. & Thorp, H.H. (1995). Kinetics and mechanism of the oxidation of sugars and nucleotides by oxoruthenium(IV): model studies for predicting cleavage patterns in polymeric DNA and RNA. *J. Am. Chem. Soc.* **117**, 1463-1471.
17. Norden, B., Lincoln, P., Akerman, B. & Tuite, E. (1996). DNA interactions with substitution-inert transition metal ion complexes. *Metal Ions. Biol. Syst.* **33**, 177-252.
18. Pyle, A.M., Rehmann, J.P., Meshoyrer, R., Kumar, C.V., Turro, N.J. & Barton, J.K. (1989). Mixed-ligand complexes of ruthenium(II). *J. Am. Chem. Soc.* **111**, 3051-3058.
19. Kalsbeck, W.A. & Thorp, H.H. (1993). Determining binding constants of metal complexes by quenching of the emission of $Pt_2(pop)_4^{4-}$. *J. Am. Chem. Soc.* **115**, 7146-7151.
20. Satyanarayana, S., Dabrowiak, J.C. & Chaires, J.B. (1993). Tris(phenanthroline)ruthenium(II) enantiomer interactions with DNA: mode and specificity of binding. *Biochemistry* **32**, 2573-2584.
21. Neyhart, G.A., Grover, N., Smith, S.R., Kalsbeck, W.A., Fairley, T.A., Cory, M. & Thorp, H.H. (1993). Binding and kinetics studies of oxidation of DNA by oxoruthenium(IV). *J. Am. Chem. Soc.* **115**, 4423-4428.
22. Kalsbeck, W.A. & Thorp, H.H. (1994). Role of the buffer cation in determining binding constants for metal complexes to DNA. *Inorg. Chem.* **33**, 3427-3429.
23. Rouault, T.A. & Klausner, R.D. (1996). Post-transcriptional regulation of genes of iron metabolism in mammalian cells. *J. Biol. Inorg. Chem.* **1**, 494-499.
24. O'Halloran, T. (1993). Transition metals in control of gene expression. *Science* **261**, 715-725.
25. Theil, E. (1998). The iron responsive element (IRE) family of mRNA regulators. *Metal Ions Biol. Syst.* **35**, 403-433
26. Ke, Y., Wu, J., Leibold, E.A., Walden, W.E. & Theil, E.C. (1998). Loops and bulge/loops in iron responsive element (IRE) isoforms influence iron regulatory protein (IRP) binding: fine-tuning of mRNA regulation. *J. Biol. Chem.*, in press.
27. Gdaniec, Z., Sierzputowska-Gracz, H. & Theil, E.C. (1998). Iron regulatory element and internal loop/bulge structure for ferritin mRNA studied by cobalt(III) hexammine binding, molecular modeling, and NMR spectroscopy. *Biochemistry* **37**, 1505-1513.
28. Laing, L.G. & Hall, K.B. (1996). A model of the iron responsive element RNA hairpin loop structure determined from NMR and thermodynamic data. *Biochemistry* **35**, 13586-13596.
29. Addess, K.J., Basilion, J.P., Klausner, R.D., Rouault, T.A. & Pardi, A. (1997). Structure and dynamics of the IRE RNA: implications for binding of the RNA by IREPs. *J. Mol. Biol.* **274**, 72-83.
30. Mathews, D.H., Andre, T.C., Kim, J., Turner, D.H. & Zuker, M. (1998). An updated recursive algorithm for RNA secondary structure prediction with improved thermodynamic parameters. *ACS Symp. Ser.* **682**, 246-257.
31. Rouault, T.A., Hentze, M.W., Caughman, S.W., Harford, J.B. & Klausner, R.D. (1988). Binding of a cytosolic protein to the IREn-responsive element of human ferritin messenger RNA. *Science* **241**, 1207-1210.
32. Henderson, B.R., Menotti, E., Bonnard, C. & Kuhn, L.C. (1994). Optimal sequence and structure of iron-responsive elements. *J. Biol. Chem.* **269**, 17481-17489.
33. Harrell, C.M., McKenzie, A.K., Patino, M.M., Walden, W.E. & Theil, E.C. (1991). Ferritin mRNA: interactions of iron regulatory element with translational regulator protein P-90 and the effect of base-paired flanking regions. *Proc. Natl Acad. Sci. USA* **88**, 4166-4170.
34. Butt, J., *et al.*, & Rouault, T.A. (1996). Differences in the RNA binding sites of iron regulatory proteins and potential target diversity. *Proc. Natl Acad. Sci. USA* **93**, 4345-4349.
35. Hentze, M.W., Rouault, T.A., Harford, J.B. & Klausner, R.D. (1989). Oxidation-reduction and the molecular mechanism of a regulatory RNA-protein interaction. *Science* **244**, 357-359.
36. Dix, D.J., Lin, P.-N., McKenzie, A.R., Walden, W.E. & Theil, E.C. (1993). The influence of the base-paired flanking region of structure and function of the ferritin mRNA iron regulatory element. *J. Mol. Biol.* **231**, 230-240.
37. Wang, Y.-H., Sczekan, S.R. & Theil, E.C. (1990). Structure of the 5'-untranslated regulatory region of ferritin mRNA studied in solution. *Nucleic Acids. Res.* **18**, 4463-4468.
38. Lim, A.C. & Barton, J.K. (1993). Chemical probing of tDNAphe with transition metal complexes: a structural comparison of RNA and DNA. *Biochemistry* **32**, 11029-11034.
39. Holmes, C.E. & Hecht, S.M. (1993). Fe•bleomycin cleaves a transfer RNA precursor and its "transfer DNA" analog at the same major site. *J. Biol. Chem.* **268**, 25909-25913.
40. Kappen, L.S. & Goldberg, I.H. (1994). Bulge-specific cleavage in transactivation response region RNA and its DNA analogue by neocarzinostatin chromophore. *Biochemistry* **34**, 5997-6002.
41. Sierzputowska-Gracz, H., McKenzie, R.A. & Theil, E.C. (1995). The importance of a single G in the hairpin loop of the iron responsive element (IRE) in ferritin mRNA for structure: an NMR spectroscopy study. *Nucleic Acids Res.* **23**, 146-153.
42. Ciftan, S.A., Hondros, D.P. & Thorp, H.H. (1998). Quenching of guanine oxidation by oxoruthenium(IV): effects of divalent cations on chemical nuclease studies. *Inorg. Chem.* **37**, 1598-1601.
43. Chen, X., Woodson, S.A., Burrows, C.J. & Rokita, S.E. (1993). A highly sensitive probe for guanine N7 in folded structures of RNA: application to tRNAphe and Tetrahymena group I intron. *Biochemistry* **32**, 7610-7616.
44. Chow, C.S., Behlen, L.S., Uhlenbeck, O.C. & Barton, J.K. (1992). Recognition of tertiary structure in tRNAs by $Rh(phen)_2(phi)^{3+}$, a new reagent for RNA structure-function mapping. *Biochemistry* **31**, 972-982.
45. Murakawa, G.J., Chen, C.B., Kuwabara, M.D., Nierlich, D.P. & Sigman, D.S. (1989). Scission of RNA by the chemical nuclease of 1,10-phenanthroline-copper ion: preference for single-stranded loops. *Nucleic Acids Res.* **17**, 5361-5375.
46. Huettenhofer, A. & Noller, H.F. (1994). Footprinting mRNA-ribosome complexes with chemical probes. *EMBO J.* **13**, 3892-3901.
47. Weeks, K.M. & Cech, T.R. (1995). Protein facilitation of group I intron splicing by assembly of the catalytic core and the 5' splice site domain. *Cell* **82**, 221-227.
48. Hickerson, R.P., Watkins-Sims, C.D., Burrows, C.J., Atkins, J.F., Gesteland, R.F. & Felden, B. (1998). A nickel complex cleaves uridine in folded RNA structures: application to *E. coli* tmRNA and related engineered molecules. *J. Mol. Biol.* **279**, 577-587.
49. Chen, X., *et al.*, & Varmus H.E. (1995). Structural and functional studies of retroviral RNA pseudoknots involved in ribosomal frameshifting: nucleotides at the junction of the two stems are important for efficient ribosomal frameshifting. *EMBO J.* **14**, 842-852.
50. Butcher, S.E. & Burke, J.M. (1994). Structure-mapping of the hairpin ribozyme. Magnesium-dependent folding and evidence for tertiary interactions within the ribozyme-substrate complex. *J. Mol. Biol.* **244**, 52-63.
51. Mazumder, A., Chen, C.-H.B., Gaynor, R. & Sigman, D.S. (1992). 1,10-phenanthroline-copper, a footprinting reagent for single-stranded regions of RNAs. *Biochem. Biophys. Res. Commun.* **187**, 1503-1509.
52. Gold, L., Polisky, B., Uhlenbeck, O. & Yarus M. (1995). Diversity of oligonucleotide functions. *Annu. Rev. Biochem.* **64**, 763-797.

Because *Chemistry & Biology* operates a 'Continuous Publication System' for Research Papers, this paper has been published via the internet before being printed. The paper can be accessed from http://biomednet.com/cbiology/cmb – for further information, see the explanation on the contents pages.